

Contents lists available at ScienceDirect

Journal of Physics and Chemistry of Solids

journal homepage: www.elsevier.com/locate/jpcs





Mapping the dispersion of the occupied and unoccupied band structure in photoexcited 1T-TiSe₂

Maximilian Huber ^a, Yi Lin ^a, Nicholas Dale ^{a,b}, Renee Sailus ^c, Sefaattin Tongay ^c, Robert A. Kaindl ^{a,d}, Alessandra Lanzara ^{a,b,*}

- ^a Materials Science Division, Lawrence Berkeley National Laboratory, Berkeley, CA, 94720, USA
- ^b Physics Department, University of California Berkeley, Berkeley, CA, 94720, USA
- ^c Materials Science and Engineering Department, Arizona State University AZ 85281, USA
- ^d Department of Physics and CXFEL Labs, Arizona State University, AZ, 85287, USA

ABSTRACT

Charge density waves (CDW) are states of broken symmetry with a periodic modulation of charge and lattice typically leading to the opening of a gap in the band structure. In the model CDW system 1T- $TiSe_2$ such a gap opens up between its Se_{4p} valence and Ti_{3d} conduction band, accompanied by a change of dispersion. These changes are crucial in understanding the CDW phase, as they provide a measure of the Se_{4p} - Ti_{3d} hybridization strength and characteristic mechanistic features. Using time- and angle-resolved photoelectron spectroscopy (trARPES), the unoccupied band structure is populated with near-infrared (NIR) pump pulses which allows to directly visualize the parabolically-shaped Ti_{3d} conduction band. Furthermore, we observe a transient change of effective mass in the Se_{4p} valence band following photoexcitation. This occurs alongside an overall reduction due to weakening of the CDW phase and is accompanied by an oscillating component with the frequency of the characteristic A_{1g} phonon. These observations, enabled by trAPRES, highlight the importance of the lattice contributions in establishing the CDW order in 1T- $TiSe_2$.

1. Introduction

The question of the origin of the charge-density wave (CDW) state in 1T-TiSe₂ remains up to now puzzling and is topic of recent research. It is commonly accepted that the CDW phase is stabilized by a combination of the pseudo Jahn-Teller effect and excitonic insulator mechanism [1], however the exact interplay of both effects remains elusive. Equilibrium studies have mostly suggested a pseudo Jahn-Teller effect [2–5], strongly supported by the observed phonon softening [6,7] although an excitonic mechanism has also been proposed, based on the report of plasmon softening [8]. The latter scenario is further supported by time-resolved studies, where an ultrafast melting of CDW order [9–11] at high excitation densities has been reported, whose timescale and fluence scaling are suggestive of an electronically mediated CDW phase.

Angle resolved photoemission spectroscopy (ARPES) is the ideal tool to study charge density wave order and many-body interactions, as it provides direct access to the quasiparticle band structure. The combination with a pump beam in a time resolved ARPES (trARPES) setup allows to populate in equilibrium unoccupied states and study photo-induced dynamics of excited carriers and scattering processes [11–13].

In this work we use extreme-ultraviolet (XUV) trARPES [14] to study the dispersion of the band structure above the Fermi level as well as the Se4p valence band at Γ point. We find that optical excitation populates a second parabolically-shaped branch of the conduction band which we associate with the Ti_{3d} band. Additionally, at the Γ point, we reveal oscillations of the Se4p valence band position at a frequency comparable with the A_{1g} phonon characteristic of the CDW phase. These oscillations can be only seen at the top of the valence band, hinting towards a transient change of dispersion and effective mass renormalization, thus exemplifying the importance that Jahn-Teller interactions also play in establishing CDW order.

2. Results and discussion

Fig. 1 shows the dynamics of the electronic band structure at the M and Γ point upon pump excitation along the high symmetry direction, Γ – M (see Fig. 1a). Data are taken in the CDW state, for T=80 K and at a fluence of $80~\mu J/cm^2$. Fig. 1a shows the 2D Brillouin zone (BZ) in the high symmetry (orange) and CDW (black) state. When going through the phase transition, the unit cell size doubles from a $(1 \times 1 \times 1)$ structure at

Abbreviations: trARPES, time resolved ARPES; CDW, Charge Density Waves.

^{*} Corresponding author. Materials Science Division, Lawrence Berkeley National Laboratory, Berkeley, CA, 94720, USA. *E-mail address:* alanzara@lbl.gov (A. Lanzara).

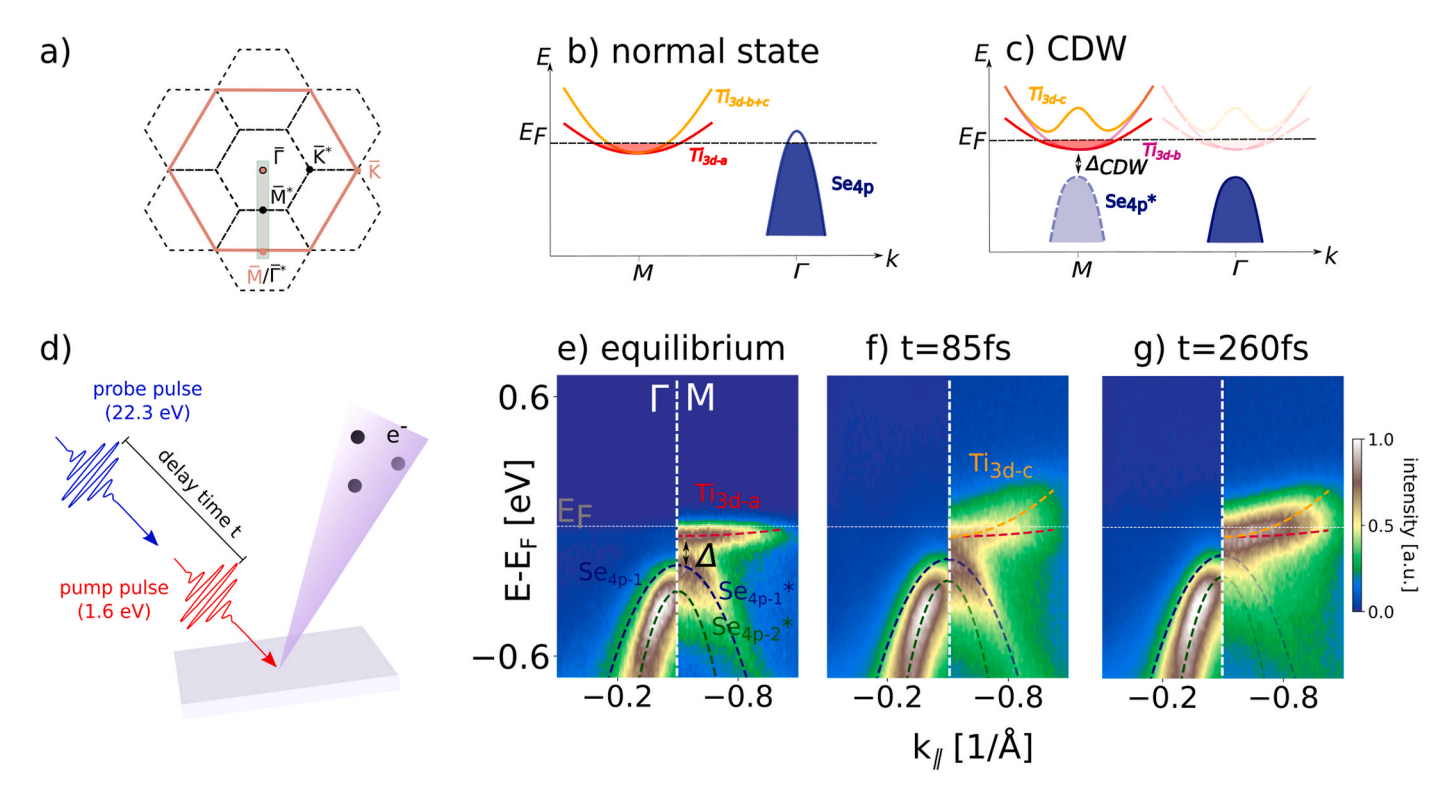


Fig. 1. a) First BZ in the high symmetry (orange) and CDW phase (black); the grey bar illustrates the cuts measured in the ARPES spectra in Γ-M direction. b-c) Schematic band structure [15] of the (b) high symmetry as well as (c) CDW state. Note that in both phases three Ti_{3d} bands are present with their center being threefold degenerate in the high symmetry phase. d) Schematic representation of a trARPES experiment. Pump pulses with 1.6 eV excite the sample, which is subsequently probed by 22.3 eV XUV probe pulses. e-g) ARPES spectra of the Γ and M-point at 80 K in equilibrium (e) and after excitation with 780 nm pump pulses at 80 μ J/cm² after 85 fs (f) and after 260 fs (g). The Fermi level is indicated by the dashed grey line.

room temperature to a $(2 \times 2 \times 2)$ superstructure below ~200 K [16]. Fig. 1b and c shows a schematic of the calculated band structure -adapted from Ref. [15]- corresponding respectively to the high symmetry and CDW state at Γ and M point with a focus on the Ti_{3d} conduction and the Se_{4p} valence band. We note that the Se_{4p} band, derived from Se $4p_{x,y}$ [3] orbitals, is spin-orbit split into two individual bands, Se_{4p-1} and Se_{4p-2}, which was neglected in this calculation. Fingerprints of the CDW state are the backfolding of the Se_{4p} bands onto the M point Se_{4p}^* and the opening of a gap [2-4,9,17]. While the gap is formed between the lowest conduction band, the Ti_{3d-a} band, and the upper Se_{4p-1}* band, the former does not interact with the Se band and remains unchanged in both the high and low temperature phase [15,18]. Instead it is the Ti_{3d-c} band that hybridizes with the center of the Se_{4p} band [19, 20]. A schematic representation of our experiment is given in Fig. 1d. NIR Pump pulses with 780 nm (~1.6 eV) excite the sample at 80 K, which is then subsequently probed by 22.3 eV XUV probe pulses. The angle and energy of the photoemitted electrons are detected with a hemispherical analyzer. Details to the setup can be found in Ref. [14]. Raw energy vs momentum maps are shown in Fig. 1e-g at equilibrium and for different delay times. At equilibrium (Fig. 1e), although both

spin-orbit split Se_{4p} bands are resolved, matrix element effects allow us to visualize them one at a time. Specifically at the M point we can clearly resolve the Se_{4p-1} band while the Se_{4p-2} is better visible at the Γ point. We can additionally resolve the bottom of the Ti_{3d-a} conduction band at the M point and hence access the CDW gap (Δ). A number of clearly visible changes in the excited state (Fig. 1f and g) can be observed in agreement with earlier work [9,11,13,14]. This includes (i) population of states above the Fermi level by hot electrons, in particular the occupancy of the previously unoccupied parabolic band, which we assign tentatively to Ti_{3d-c} (compare Fig. 1b and c); (ii) a partial closing of the gap between the Ti_{3d-a} and Se_{4p-1} states (Fig. 1f) at M, accompanied by (iii) an upshift of the Se_{4p-2} band at Γ and (iv) the disappearance of the Se_{4p-1} backfolded band at M in concomitance with the gap closing at later delay time (t=260 fs, Fig. 1g).

To study the excited states in more detail, we present in Fig. 2 ARPES maps near the Fermi level which were averaged over extened measurement times. The photoexcited data at 100 fs is shown in Fig. 2a alongside with its second derivative in Fig. 2b. These data reveal that a significant amount of hot electrons occupy states above the Fermi level in what resembles an upwards-facing -electron-like- parabola in

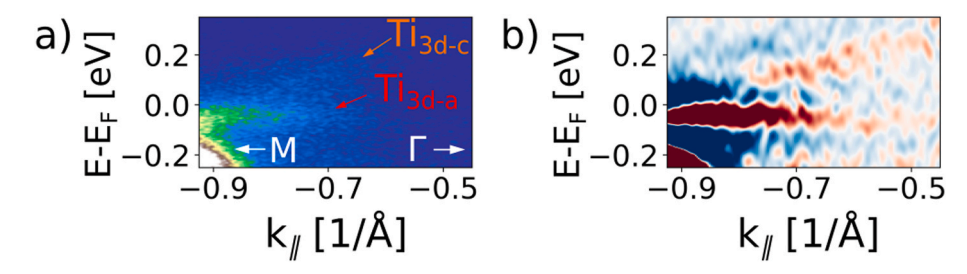


Fig. 2. a) ARPES image plot after excitation with 70 μ J/cm² after 100 fs b) Corresponding second derivative image after smoothing with the Gaussian method over a window of 30 meV.

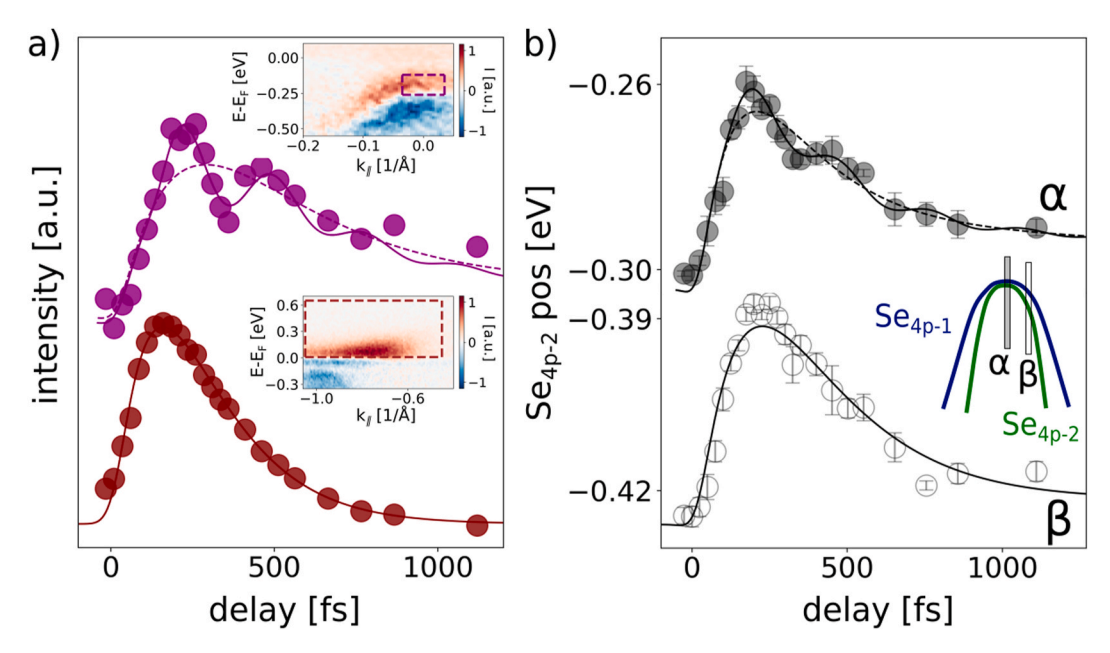


Fig. 3. a) Dynamics of the intensity integrated above the Se_{4p-2} band (magenta, integration region shown in the inset) versus the dynamics of excited carriers (red, integration region see inset) after excitation with 80 $\mu J/cm^2$. Solid lines are fits to the data. b) Momentum resolved dynamics of the Se_{4p-2} position after excitation with 80 $\mu J/cm^2$. Solid lines are fits to the data. Curve *α* was obtained by fitting EDCs taken right at Γ point, curve *β* from EDCs taken at $k_{\parallel} = -0.1 \text{ Å}^{-1}$. The integration regions for the EDCs is schematically depicted in the inset.

accordance with Fig. 1e–g. This newly populated orbital is different from the less-dispersing, in equilibrium partially occupied ${\rm Ti}_{3d\text{-}a}$ orbital. Moreover, the expectation that the ${\rm Ti}_{3d\text{-}a}$ orbital should not considerably change its shape [15,18,21], as it barely hybridizes with the ${\rm Se}_{4p}$ valence band or shift upwards during the phase transition to the high temperature state [22] implies that another orbital which is distinct from ${\rm Ti}_{3d\text{-}a}$ gets transiently populated. This cannot be the ${\rm Ti}_{3d\text{-}b}$ band which should carry negligible spectral weight [15]. Therefore we assign this band to the ${\rm Ti}_{3d\text{-}c}$ band [15,18], which hybridizes with the Se valence band and is thus sensitive to CDW formation. From Fig. 2a it appears like the ${\rm Ti}_{3d\text{-}a}$ and ${\rm Ti}_{3d\text{-}c}$ bands are merging into each other at M point, however we note that for this pump fluence the CDW phase gets strongly perturbed, i. e. the splitting between the bands is significantly reduced and is thus most likely simply too small to be resolved in our experiment.

Our ability to resolve this band constitutes the first step toward a more complete understanding of the mechanism behind the CDW transition in TiSe2. Indeed, in a Jahn-Teller scenario the degeneracy of the bottom of the parabolic-like ${\rm Ti}_{3d\text{-}a}$ and ${\rm Ti}_{3d\text{-}c}$ is lifted [2,18], leading to an upshift of the hybridising ${\rm Ti}_{3d\text{-}c}$ center. On the other hand, within an excitonic insulator scenario more pronounced changes of the band structure are expected [15,23], with the presence of a characteristic double-well shape predicted by Kohn in his seminal work [24]. In general, however, it is a very delicate task to observe bands above the Fermi level corresponding to the CDW state experimentally, since the commonly used 780 nm pump wavelength mostly excites electrons high above the Fermi level [13,25]. Thus, by the time these carriers scatter down to lower energies, the CDW phase is already strongly perturbed or quenched, thus displaying the high symmetry band structure. Further studies using high resolution XUV-trARPES systems with MIR pump could potentially solve these problems, driving a direct excitation into the Ti_{3d-c} orbital [26] which could provide clear evidence for a Mexican hat shaped conduction band.

We now focus our attention to the dynamical evolution of the Se_{4p} valence band following photo-excitation. As the intensity of this band at Γ point stays constant over all delays, integrating slightly above the position of the band maximum in equilibrium can give information about transient band shifts following optical excitation. In Fig. 3a we show this integrated spectral weight, with the integration region

indicated in the difference spectrum in the inset. In addition to the sudden increase of intensity following photoexcitation, the data also reveal an oscillating component as a function of delay time. To best describe the dynamical evolution of the data over time we thus use a fitting function consisting of three exponentials (one describing the rise time and a fast and slow component for the recovery time [13]) as well as a damped cosine function convoluted with a Gaussian accounting for the experimental time resolution. We find an oscillation frequency of 3.48 \pm 0.24 THz, which is comparable to the A_{1g} phonon mode characteristic of the CDW state [27]. In contrast, the intensity of the excited carriers shows only a sudden increase followed by a fast decrease without any sign of oscillations.

In Fig. 3b we study the time delay dependence of the valence band energy position. To extract the energy vs momentum position of the valence band, EDCs were fitted using two peaks of Voigt lineshape on a linear background (accounting for the Se_{4p-2} and a Se_{4p-2} [23] band). The position of the Se_{4p-2} peak position at the band maximum at $k_{\parallel} = 0 \text{ Å}^{-1}$ (i. e. Γ point, denoted as α), reveal an overall upshift of the band followed by a downshift to slightly above the equilibrium position at later delay times. The upshift of the valence band is indicative of a partial closing of the gap, suggesting a weakening of the CDW phase. A closer look reveals that the valence band position also shows an oscillating component. The frequency of the oscillation is similar to the one observed for the Se_{4p} intensity, with frequencies of 3.40 \pm 0.47 THz and 3.48 \pm 0.24 THz, comparable to the phonon mode frequency and thus implying a strong intrinsic coupling between the atomic motion and the electronic structure [26]. To better understand the changes in the band structure due to the oscillations, in Fig. 3b we show the Se_{4p-2} peak position away from the maximum of the Se_{4p} band at $k_{\parallel}=-0.1\,\mathring{\mathrm{A}}^{-1}$ (denoted as β) as a function of the delay time. Interestingly, the position shows an overall upward shift towards the Fermi level similar to the one observed at α , reaching its maximum at the same time and then slowly decaying back toward equilibrium without any oscillation, in contrast to the behavior of the band maximum position α . The different response of the top (α) and side (β) of the Se_{4p} band to photoexcitation suggests a transient change of effective mass, probably with this phonon frequency.

Motivated by these results, in Fig. 4 we analyze the dispersion of the selenium valence band in more detail to directly extract information on

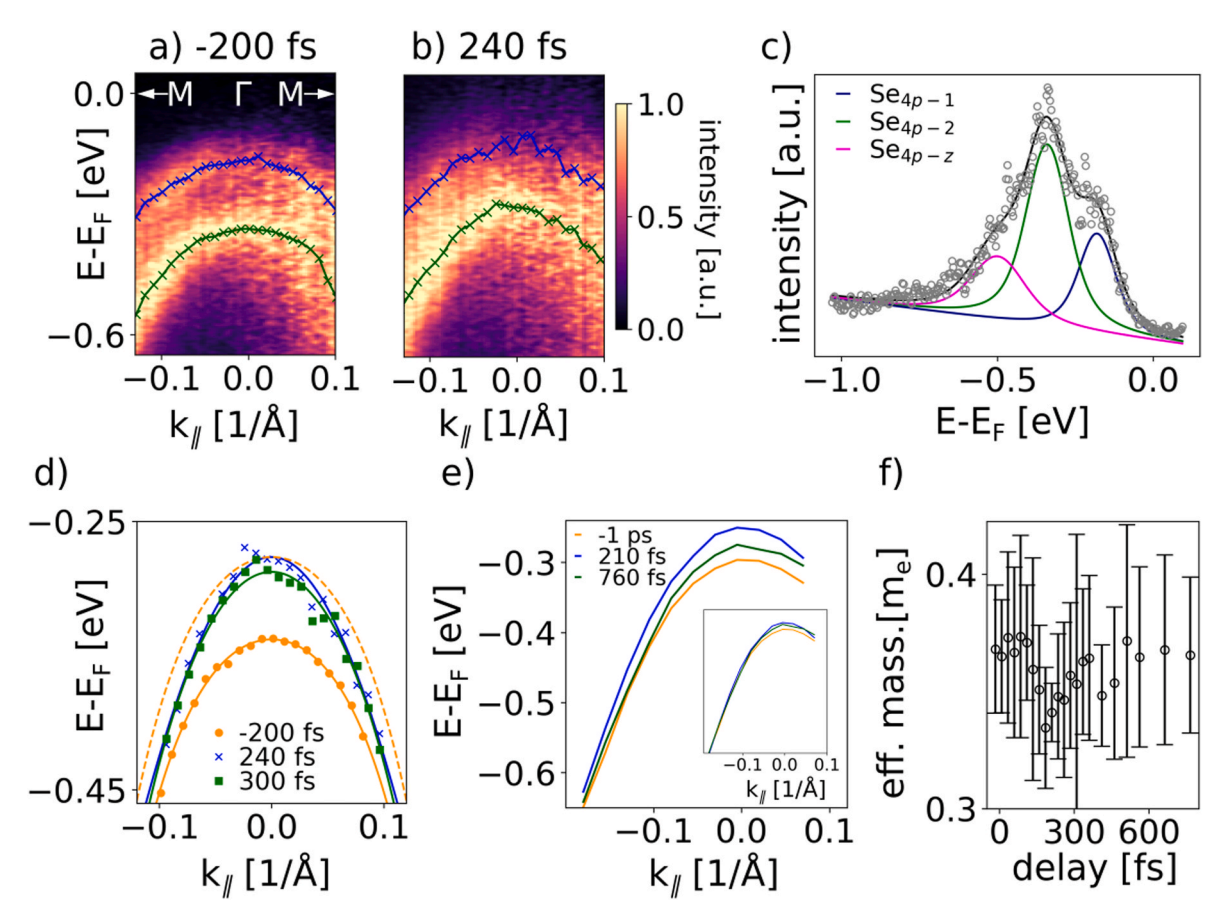


Fig. 4. a-b) ARPES maps around the Γ-point (a) before excitation and (b) 240 fs after excitation with 90 $\mu J/cm^2$ pump fluence. In order to compensate for matrix element effects spectra are normalized so that every EDC slice carries the same maximum and minimum intensity. The fitted band position for the Se_{4p-1} and Se_{4p-2} band are shown in blue and green, respectively. c) EDC for a time delay of t = -200 fs at momentum $k_{\parallel} = 0$ Å⁻¹ along with fits. d) Se_{4p-2} band dispersion extracted from fitting EDCs at t = -200 fs (orange), 240 fs (blue) and 300 fs (green) after excitation with 90 $\mu J/cm^2$. Solid lines are fits to the data using a fourth order polynomial. For a direct comparison a copy of the orange line is shifted upward in energy. e) Se_{4p-2} band dispersion extracted from fitting EDCs at t = -1 ps (orange), 210 fs (blue) and 760 fs (green) after excitation with 80 $\mu J/cm^2$ fluence. The inset shows the same bands but shifted in energy so that the band positions at -0.15 Å⁻¹ are aligned. f) Effective mass of the Se_{4p-2} band after excitation with 80 $\mu J/cm^2$ extracted from parabolic fits to the dispersion.

the effective mass. Fig. 4a-b shows the transient ARPES map around Γ before excitation (t = -200 fs) and for t = 240 fs after excitation with a fluence of 90 $\mu J/cm^2$, respectively. For this sample, both spin-orbit split Se bands can be clearly identified. This is clear in the EDCs (Fig. 4c) where one can easily distinguish the two peaks at about -0.18 eV, -0.32 eV as well as a shoulder at -0.5 eV, which are, respectively, attributed to the Se_{4p-1} , Se_{4p-2} and Se_{4p-3} orbitals [23]. To enhance clarity and compensate for matrix-element effects we normalize the intensity of the spectrum for each energy position. The fitted band positions of both Se_{4p-1} and Se_{4p-2} band over momentum space are superimposed in blue and green markers, respectively. One can clearly see that both bands shift significantly up in energy after optical excitation while simultaneously becoming more parabolic, indicative of a decrease of effective mass. To make the change in band dispersion clearer, in Fig. 4d plots the extracted band dispersion of the Se_{4p-2} valence band before excitation and in the excited state at two different delays. To describe the dispersion over a broad momentum range, we fit the data points with a fourth-order polynomial. Between -200 fs (orange data points) and 240 fs (blue data points) the whole band shifts up about 55 meV, accompanied by a clear change of effective mass. For a direct comparison we shifted the fitted dispersion of the equilibrium band dispersion up to the position of the excited band (dotted orange line). Interestingly, between 240 and 300 fs the center of the Se_{4p-2} band ($k_{\parallel} \sim -0.07$ to 0.07) is shifted slightly downward, while the edges of the band are almost at the same position, resulting in an increase of effective mass. This indicates that the changes of effective mass at the band center are

decoupled form the overall band shift. Having established this clear change in effective mass, we analyze the dispersion of the Se valence band from the dataset shown in Figs. 1 and 3 in more detail. Fig. 4e shows the extracted dispersion at three different time delays, shown over a larger momentum range than in Fig. 4d. The inset shows the same plots shifted in energy so that the band edges at $-0.15~\text{Å}^{-1}$ are aligned, showing again how the top of the band becomes modulated in a different way than the band edges away form the center, thus further reproducing the results of Fig. 4d. In Fig. 4f we show the dynamical evolution of the effective mass, extracted from parabolic fits to the band dispersion between -0.15 and $0.08~\text{Å}^{-1}$. A systematic decrease of the effective mass followed by a partial recovery can be observed.

The decrease of effective mass corresponding to the perturbation of the CDW phase is consistent with both the screening of excitons in an excitonic insulator scenario [15,23] and a weakening of the hybridization between Se_{4p} and Ti_{3d} states in a Jahn-Teller scenario [2,4,18]. On the other hand, the oscillations of the Se_{4p} band at the A_{1g} phonon frequency are a unique signature of the Jahn-Teller effect. Indeed, within an excitonic insulator scenario the dynamics of the excited carriers should be similar to the dynamics of the band structure. The absence of oscillation on the former support the role of the lattice in defining the Se_{4p} band shape. Therefore, the observed flattening of the Se_{4p} band when going from high temperature to CDW phase is very likely connected to the lattice. Nevertheless, while our results point towards the important role the Jahn-Teller effect plays in establishing CDW order they do not exclude that strong electronic correlations are present as

well. Indeed, in theoretical work it is predominantly proposed that a cooperative mechanism between both concepts is likely responsible for the formation of the low temperature CDW phase [28–30].

3. Conclusion

In conclusion, the results here presented show that the plethora of effects observed in ${\rm TiSe_2}$ provides a unique platform for studying the intriguing interplay of many-body couplings in a strongly correlated system. In this regard we observed how the effective mass, indicative of the ${\rm Se_{4p}\text{-}Ti_{3d}}$ hybridization strength decreases after optical excitation while the dispersion is modulated by phonon oscillations. This emphasizes the role that Jahn-Teller interactions play in the establishment of CDW order in ${\rm TiSe_2}$. Finally, we were also able to resolve sides of the ${\rm Ti}_{3d\text{-}c}$ band above the Fermi level.

Data availability

The datasets generated and/or analyzed during the current study are not publicly available as they contain additional findings not reported in this manuscript, but are available from the corresponding author upon reasonable request.

Author contributions

A.L. designed and supervised the project. Data was collected by M.H. and Y.L. and analyzed by M.H. with help from Y.L., N.D., R.K. and A.L. Samples were provided by R.S. and S.T. The XUV-trARPES setup was designed by R.K. Manuscript preparation was done by M.H. with input from all co-authors.

Declaration of competing interest

The authors declare that they have no known competing financial interests or personal relationships that could have appeared to influence the work reported in this paper.

Acknowledgments

This work was primarily funded by the U.S. Department of Energy (DOE), Office of Science, Office of Basic Energy Sciences, Materials Sciences and Engineering Division under contract no. DE-AC02-05CH11231 (Ultrafast Materials Science program KC2203). S.T. Acknowledges support from NSF-DMR 2111812 and NSF CMMI 1933214 for material development and characterization.

References

- [1] M. Porer, U. Leierseder, J.M. Ménard, H. Dachraoui, L. Mouchliadis, I.E. Perakis, U. Heinzmann, J. Demsar, K. Rossnagel, R. Huber, Non-thermal separation of electronic and structural orders in a persisting charge density wave, Nat. Mater. 13 (9) (2014) 857–861.
- [2] K. Rossnagel, Suppression and emergence of charge-density waves at the surfaces of layered 1T - TiSe₂ and 1T - TaS₂ by in situ Rb deposition, New J. Phys. 12 (2010).
- [3] K. Rossnagel, L. Kipp, M. Skibowski, Charge-density-wave phase transition in (formula presented): excitonic insulator versus band-type Jahn-Teller mechanism, Phys. Rev. B Condens. Matter 65 (23) (2002) 1–7.
- [4] K. Rossnagel, On the origin of charge-density waves in select layered transitionmetal dichalcogenides, J. Phys. Condens. Matter 23 (21) (2011).
- [5] A. Wegner, J. Zhao, J. Li, J. Yang, A.A. Anikin, G. Karapetrov, D. Louca, U. Chatterjee, Evidence for breathing-type pseudo Jahn-Teller distortions in the charge density wave phase of 1T-TiSe₂, Phys. Rev. B 101 (2020) 1–6.
- [6] M. Holt, P. Zschack, H. Hong, M.Y. Chou, T.C. Chiang, X-ray studies of phonon softening in TiSe₂, Phys. Rev. Lett. 86 (17) (2001) 3799–3802.

- [7] F. Weber, S. Rosenkranz, J.P. Castellan, R. Osborn, G. Karapetrov, R. Hott, R. Heid, K.P. Bohnen, A. Alatas, Electron-phonon coupling and the soft phonon mode in TiSe₂, Phys. Rev. Lett. 107 (26) (2011) 1–5.
- [8] A. Kogar, M.S. Rak, S. Vig, A.A. Husain, F. Flicker, Y.I. Joe, L. Venema, G. J. Macdougall, T.C. Chiang, E. Fradkin, J.V. Wezel, P. Abbamonte, Signatures of exciton condensation in a transition metal dichalcogenide, Science 1317 (December) (2017) 1314–1317.
- [9] T. Rohwer, S. Hellmann, M. Wiesenmayer, C. Sohrt, A. Stange, B. Slomski, A. Carr, Y. Liu, L.M. Avila, M. Kalläsignne, S. Mathias, L. Kipp, K. Rossnagel, M. Bauer, Collapse of long-range charge order tracked by time-resolved photoemission at high momenta, Nature 471 (7339) (2011) 490–494.
- [10] S. Hellmann, T. Rohwer, M. Kalläne, K. Hanff, C. Sohrt, A. Stange, A. Carr, M. M. Murnane, H.C. Kapteyn, L. Kipp, M. Bauer, K. Rossnagel, Time-domain classification of charge-density-wave insulators, Nat. Commun. 3 (2012).
- [11] S. Mathias, S. Eich, J. Urbancic, S. Michael, A.V. Carr, S. Emmerich, A. Stange, T. Popmintchev, T. Rohwer, M. Wiesenmayer, A. Ruffing, S. Jakobs, S. Hellmann, P. Matyba, C. Chen, L. Kipp, M. Bauer, H.C. Kapteyn, H.C. Schneider, K. Rossnagel, M.M. Murnane, M. Aeschlimann, Self-amplified photo-induced gap quenching in a correlated electron material, Nat. Commun. 7 (2016) 1–8.
- [12] C.L. Smallwood, J.P. Hinton, C. Jozwiak, W. Zhang, J.D. Koralek, H. Eisaki, D. H. Lee, J. Orenstein, A. Lanzara, Tracking Cooper pairs in a cuprate superconductor by ultrafast angle-resolved photoemission, Science 336 (6085) (jun 2012) 1137–1139.
- [13] M. Huber, Y. Lin, N. Dale, R. Sailus, S. Tongay, R. Kaindl, and A. Lanzara, Revealing the order parameter dynamics of 1T-TiSe₂ following optical excitation, (submitted) for publication.
- [14] J.H. Buss, H. Wang, Y. Xu, J. Maklar, F. Joucken, L. Zeng, S. Stoll, C. Jozwiak, J. Pepper, Y.-d. Chuang, J.D. Denlinger, Z. Hussain, A. Lanzara, R.A. Kaindl, A setup for extreme-ultraviolet ultrafast angle-resolved photoelectron spectroscopy at 50-kHz repetition rate, 90, 2019, 023105.
- [15] C. Monney, H. Cercellier, F. Clerc, C. Battaglia, E.F. Schwier, C. Didiot, M. G. Garnier, H. Beck, P. Aebi, H. Berger, L. Forró, L. Patthey, Spontaneous exciton condensation in 1T TiSe₂: BCS-like approach, Phys. Rev. B Condens. Matter 79 (4) (2009) 1–11.
- [16] F.J. Di Salvo, D.E. Moncton, J.V. Waszczak, Electronic properties and superlattice formation in the semimetal TiSe₂, Phys. Rev. B 14 (10) (nov 1976) 4321–4328.
- [17] T.E. Kidd, T. Miller, M.Y. Chou, T.C. Chiang, Electron-hole coupling and the charge density wave transition in TiSe₂, Phys. Rev. Lett. 88 (22) (2002) 226, 402/1–226 402/4.
- [18] M.D. Watson, O.J. Clark, F. Mazzola, I. Marković, V. Sunko, T.K. Kim, K. Rossnagel, P.D. King, Orbital- and k_z-selective hybridization of Se_{4p} and Ti_{3d} states in the charge density wave phase of TiSe₂, Phys. Rev. Lett. 122 (7) (2019) 1–6.
- [19] M. Hellgren, J. Baima, R. Bianco, M. Calandra, F. Mauri, L. Wirtz, Critical role of the exchange interaction for the electronic structure and charge-density-wave formation in TiSe₂, Phys. Rev. Lett. 119 (17) (2017) 1–6.
- [20] C. Chen, B. Singh, H. Lin, V.M. Pereira, Reproduction of the charge density wave phase diagram in 1T – TiSe₂ exposes its excitonic character, Phys. Rev. Lett. 121 (22) (2018), 226602.
- [21] R. Bianco, M. Calandra, F. Mauri, Electronic and vibrational properties of TiSe₂ in the charge-density-wave phase from first principles, Phys. Rev. B Condens. Matter 92 (9) (2015) 1–19.
- [22] C. Monney, E.F. Schwier, M.G. Garnier, N. Mariotti, C. Didiot, H. Beck, P. Aebi, H. Cercellier, J. Marcus, C. Battaglia, H. Berger, A.N. Titov, Temperature-dependent photoemission on 1T -TiSe₂: interpretation within the exciton condensate phase model, Phys. Rev. B Condens. Matter 81 (15) (2010) 1–9.
- [23] M. Cazzaniga, H. Cercellier, M. Holzmann, C. Monney, P. Aebi, G. Onida, V. Olevano, Ab initio many-body effects in TiSe₂: a possible excitonic insulator scenario from GW band-shape renormalization, Phys. Rev. B Condens. Matter 85 (19) (2012) 1–6.
- [24] W. Kohn, Excitonic phases, Phys. Rev. Lett. 19 (8) (aug 1967) 439-442.
- [25] G. Rohde, T. Rohwer, A. Stange, C. Sohrt, K. Hanff, L.X. Yang, L. Kipp, K. Rossnagel, M. Bauer, Does the excitation wavelength affect the ultrafast quenching dynamics of the charge-density wave in 1T – TiSe₂? J. Electron. Spectrosc. Relat. Phenom. 195 (2014) 244–248.
- [26] C. Monney, M. Puppin, C.W. Nicholson, M. Hoesch, R.T. Chapman, E. Springate, H. Berger, A. Magrez, C. Cacho, R. Ernstorfer, M. Wolf, Revealing the role of electrons and phonons in the ultrafast recovery of charge density wave correlations in 1T – TiSe₂, Phys. Rev. B 94 (16) (2016) 1–9.
- [27] C.S. Snow, J.F. Karpus, S.L. Cooper, T.E. Kidd, T.C. Chiang, Quantum melting of the charge-density-wave state in 1T – TiSe₂, Phys. Rev. Lett. 91 (13) (2003) 1, 364 021–1 364 024.
- [28] J. Van Wezel, P. Nahai-Williamson, S.S. Saxena, Exciton-phonon-driven charge density wave in TiSe₂, Phys. Rev. B Condens. Matter 81 (16) (2010) 1–8.
- [29] T. Kaneko, Y. Ohta, S. Yunoki, Exciton-phonon cooperative mechanism of the triple- q charge-density-wave and antiferroelectric electron polarization in TiSe₂, Phys. Rev. B 97 (15) (2018), 155131.
- [30] C. Lian, S.J. Zhang, S.Q. Hu, M.X. Guan, S. Meng, Ultrafast charge ordering by self-amplified exciton–phonon dynamics in TiSe₂, Nat. Commun. 11 (1) (2020).